RESIDUAL STRESSES IN PLASMA SPRAYED COATINGS BY X-RAY DIFFRACTOMETER

Anderson .A[1], Ramachandran .S[2]
[1]Research scholar, Department of Mechanical Engineering, Sathyabama University
[2]Department of Mechanical Engineering, Sathyabama University

Abstract

ceramic coatings are applied on various engineering hardware components to provide protection against wear, corrosion and high heat fluxes. Metal hardware operating in harsh environments could fail prematurely due to wear, corrosion and high temperature exposure. A protective layer of coating is typically applied to provide a barrier which prolongs component durability and the desired properties of the hardware components. It is widely recognized that residual stresses in thermally sprayed coatings are highly significant in practical terms. residual stress measurements obtained using X-ray diffraction techniques are in good agreement with results obtained by neutron diffraction.

Keywords:

I. INTRODUCTION

Metallic and ceramic coatings are applied on various engineering hardware components to provide protection against wear, corrosion and high heat fluxes. Metal hardware operating in harsh environments could fail prematurely due to wear, corrosion and high temperature exposure. A protective layer of coating is typically applied to provide a barrier which prolongs component durability and the desired properties of the hardware components. It is widely recognized that residual stresses in thermally sprayed coatings are highly significant in practical terms. Considerable efforts have been made in recent years to understand and predict the residual stresses that develop during the production of thermally sprayed coatings. It can be assumed that stresses in the through thickness direction are negligible and that the stresses are same in all directions within the plane of the coating.

II.PLASMA SPRAY COATINGS

Among the different coating systems, the thermal barrier coatings (TBCs) are commonly used to protect hardware operating in high temperature environments, such as combustor liners and gas turbine blades, from excessively high heat fluxes and temperatures. Among the different ceramic coating systems, yttria stabilized zirconia is widely used as thermal barrier coatings. They are conventionally applied by introducing a powder of the coating material into a plasma jet in which powder particles are melted and accelerated towards the surface to be coated. While this technology has matured over the past several decades, the recent developments have focused on attaining nanometer size features in the coating microstructure for superior coating properties in terms of better service performance and spallation resistance [1]. The processing conditions of powders for this type of coating have been recently studied in the laboratory and a pilot scale production facility [2]. Processing conditions to obtain nano-structured coatings require process optimization since the nanometer size features of the original powders need to be retained in the coating which would otherwise be lost upon melting.

While the recent studies have yielded considerable success in attaining nano-structured coatings using powders, a new method of producing nano-structured coatings was recently discovered and it involves production of nano-structured yttria stabilized zirconia coatings from liquid precursors injected into a plasma jet [3]. In this new process, schematically shown in Fig. 1, an aqueous solution of precursors (zirconium acetate, yttrium nitrate and some additives) is injected into the plasma jet in the form a spray instead of ceramic powders. Rapid heat up and evaporation of the solution droplets in the plasma jet result in the nucleation of tetragonal phase of solid yttria stabilized zirconia.

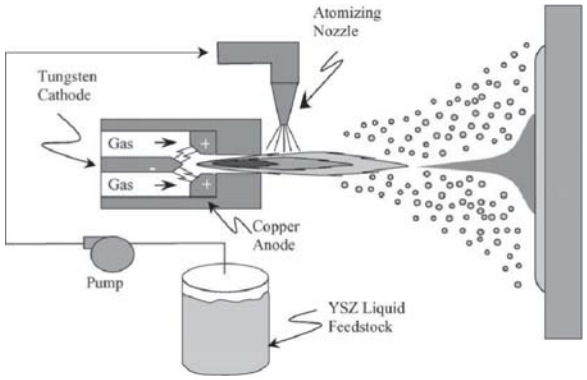

Fig. 1. Schematics of the solution precursor plasma spraying process.

The liquid precursor coating process involves injection of a liquid precursor solution in the form of a spray into a dc-arc plasma jet as shown in Fig. 1. The injected spray droplets are processed in the plasma thermal environment and are convected downstream by the

plasma flow field towards the coating location. The process involves motion of the vaporizing droplets in the plasma, vaporization of solvent (water) from the solution containing zirconium acetate (solute) as droplets traverse the plasma jet and formation of precipitates in these droplets ultimately leading to formation of zirconium oxide. In the analysis that follows, the solvent volatility is much greater than that of the zirconium acetate such that zirconium acetate remains in the droplet as water evaporates thus concentrating the solute within the droplet. The nominal values for droplet size and injection velocity were taken as 40μm and 12 m/s, respectively. The injected droplets subtend a spray cone angle of 15°.Temperature variation of ±20% of the baseline case and velocity variation of ±50% were considered.

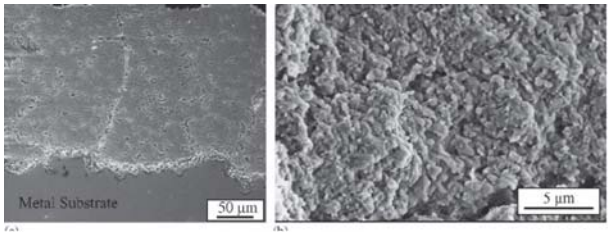

Fig. 2. SEM images of the typical morphologies obtained from solution precursor plasma spray process

Table 1. Thermophysical properties of the plasma gas Plasma properties [4]

	a	*b*	*C*
Density (kgm- 3) $\rho = a(T + b)c$	1.397 103	1.376x 10^{2}	- 1.160
Dynamic viscosity (kgm^{-1} s^{-1}) $\mu = a + bT +$	1.382 x10^{-6}	5.968 x10^{-8}	- 1.882 x10^{-11}
cT^2 Specific heat (J kg^{-1} K^{-1}) $CP = a$	9.376 x10^{2}	1.974 x10^{-1}	
$+ bT$ Thermal conductivity (Wm^{-1} K^{-1}) $k = a + bT$	1.125 x10^{-2}	5.499 x10^{-5}	

Tabulated data available in the property database [4] is curve-fitted in the temperature range of 500–7000 K.

III. RESIDUAL STRESSES

Residual (locked-in) stresses in a structural material or component are those stresses which exist in the object without (and usually prior to) the application of any service or other external loads. Manufacturing processes are the most common causes of residual stress. Virtually all manufacturing and fabricating processes -- casting, welding, machining, molding, heat treatment, etc. -- introduce residual stresses into the manufactured object. Another common cause of residual stress is in-service repair or modification. In some instances, stress may also be induced later in the life of the structure by installation or assembly procedures, by occasional overloads, by ground settlement effects on underground structures, or by dead loads which may ultimately become an integral part of the structure. The effects of residual stress may be either beneficial or detrimental, depending upon the magnitude, sign, and distribution of the stress with respect to the load-induced stresses. Very commonly, the residual stresses are detrimental, and there are many documented cases in which these stresses were the predominant factor contributing to fatigue and other structural failures when the service stresses were superimposed on the already present residual stresses. The particularly insidious aspect of residual stress is that its presence generally goes unrecognized until after malfunction or failure occurs.

IV. MEASUREMENT OF RESIDUAL STRESSES

Measurement of Residual Stresses by various methods such as the Hole-Drilling Strain Gage Method, Compliance Methods, Magnetic and Electrical Methods, Ultrasonic Methods, Thermo elastic Methods, Photo elastic Methods, Diffraction Methods.

A.1. Diffraction Methods

A.1.1.Neutron Diffraction

Neutron diffraction is a non-destructive method of determination of residual stresses in crystalline materials. Neutron diffraction provides the values of elastic strain components parallel to the scattering vector which can be converted to stress. Neutron diffraction measures strain components from changes in crystal lattice spacing. When crystalline materials exposed to radiation of wavelength close to interplanar spacing (0.5-3 Å) elastically and coherently scatter this radiation as distinctive Bragg peaks imaged usually by a position sensitive detector. The angle at which any given peak occurs can be calculated using Bragg's equation

$$2d_{hkl}\sin\theta_{hkl} = \lambda \qquad (1)$$

Where λ is the wavelength of the radiation, $d$hkl is the lattice plane spacing of a family of crystallographic planes

(*hkl*) responsible for the Bragg peak and θhkl is the angular position of this diffraction peak. The peak will be observed at an angle of 2θhkl from the incident beam. If a specimen is elastically strained, the lattice spacing changes. Therefore any elastic strain will be apparent as a shift in the value of 2θhkl for a particular reflecting plane illuminated by a fixed wavelength.

A.1.2 Synchrotron Diffraction

Synchrotrons (hard X-rays), provide very intense beams of high energy X-rays. These X-rays have higher depth penetration than conventional X-rays (~50 mm in Al). This increased penetration depth means that synchrotron diffraction is capable of providing high spatial resolution, three- dimensional maps of the strain distribution to millimeter depths in engineered components. Higher penetration depth is considered as one of the major advantages of synchrotron diffraction over the conventional X-ray diffraction. Another advantage is that intense narrow beams of 1 mm-l0 μm in size are possible. This leads to spatial resolutions that are limited by the crystallite size within the sample not by the instrument. The measurement is also much quicker than the conventional X-ray diffraction. Today synchrotron diffraction is only available at some central facilities, in much the same way as with neutron diffraction.

V. FUNDAMENTAL CONCEPTS IN X-RAY DIFFRACTION

Diffraction methods of residual stress determination basically measure the angles at which the maximum diffracted intensity take place when a crystalline sample is subjected to x-rays. From these angles it is possible to obtain the interplanar spacing of the diffraction planes using Bragg's law. If the residual stresses exist within the sample, then the d spacing will be different than that of an unstressed state. This difference is proportional to magnitude of the residual stress.

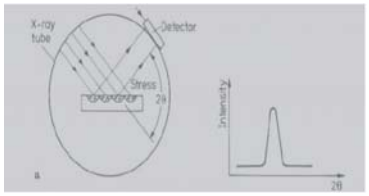

Fig. 3. Diffractometer scheme.

With reference to Figure 3, assume that the detector is turned over a range of angles, 2θ, to find the angle, θ, of the diffraction from grains which satisfy Bragg's law. In other words the grains that have planes of atoms with interplanar spacing "d" such that $\lambda = 2d\sin\theta$. The grains that have planes with this spacing that are parallel to the surface will diffract as in Figure 3. This diffraction occurs from a thin surface layer which is about 20 μm. If the surface is in compression, then the interplanar spacing "d" is larger than in the stress free state as a result of Poisson's effect. When the specimen is tilted with respect to the incoming beam new grains will diffract and the orientation of the diffraction planes is more nearly perpendicular to the stress direction (Figure 4).

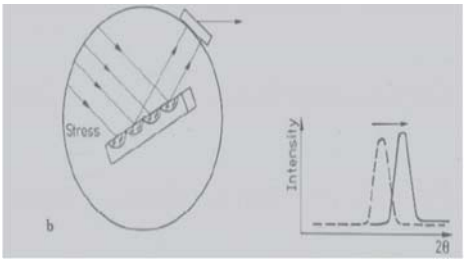

Fig. 4. When the sample is tilted, diffraction will take place from other grains, but from the same planes (that satisfy Bragg's law). The peak takes place at higher values of 2θ. [6]

As a result of the tilt, the d spacing decreases and the angle 2θ increases, as seen in the figures. In this case the d spacing acts as a strain gauge. Because of the fact that the interplanar spacing is so small, both micro and macro stresses will effect it. The XRD measures sum of all these stresses. X-rays are produced in a standard way: by accelerating electrons with a high voltage and allowing them to collide with a metal target. When a beam of x-rays is incident on the specimen, the photons collide with the electrons and scatter in different directions. There are two types of collisions. First type is elastic and the second one is inelastic. The former is the case when the x-rays collide with the electrons that are tightly bound to nucleus (usually the inner orbital electrons).

There is no momentum transfer between the photon and electron which means scattered photon has the same energy and wavelength after the collision. This type of scattering is called coherent scattering (Figure 5). On the other hand, for the inelastic collision there is a momentum transfer from photon to electron. Due to this momentum transfer, photon looses energy and has longer wavelength. When an unpolarized x-ray beam impinges on an electron, the total scattered intensity on a point P is given by the equation $I = (I_0 e^4)/(r^2 m^2 c^{4)}\{(1+\cos^2\theta)/2\}$

where I0 is the intensity of the incoming beam, m is the electron mass, c is the speed of light, e is the electron charge, r is the length of the position vector to point P, and 2θ is the angle between r and the incident beam direction. The term $(1+\cos^2 2\theta)$ is called polarization factor.

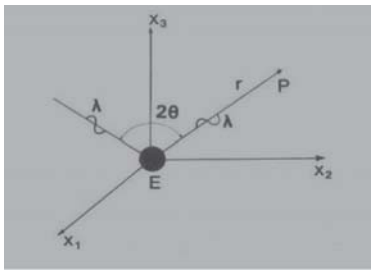

Fig. 5. Coherent scattering from an electron to a point P [6].

Experimental Techniques

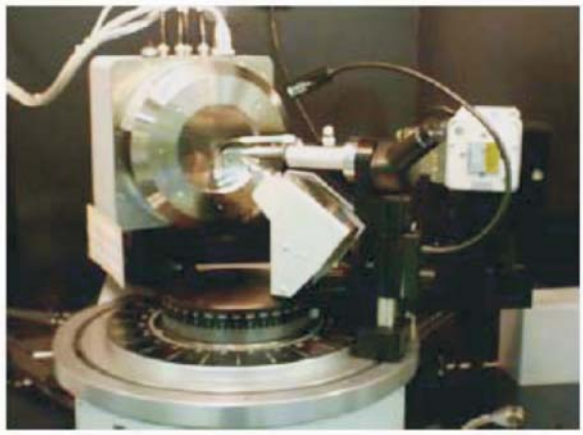

Fig. 6. Bruker-AXS GADDS 2D powder and single-crystal X-Ray diffractometer

For measurement of diffraction events from regular and irregularly shaped samples. The instrument employs;

the H-star multi-wire two-dimensional area detector (1024 x 1024 pixel size)

a Cu X-ray tube.

A small monochromatic X-ray beam is used to probe micro and irregular areas.

VI. RESULTS

The X-ray diffraction measurements are shown in Table 2. The depth at which the measurement is quoted is the sum of the polishing depth and the calculated penetration depth of the X-ray beam. For example for the measurements made at location A, the effective depth of the measurement, d can be expressed as:

d = material removed + penetration depth,

d = 0 + 0.0085 mm

The raw data and corrected values at each location are given in Table 2 with the uncertainty that has been evaluated in accordance with the NPL Good Practice Guide No. 52 [7].

Table 2. XRD Residual stress values

Location and depth (mm)	Residual Stress, MPa		
	Raw	Corrected	Uncertainty
A: 0.0085	-631	-631	±55
B: 0.0765	-877	-844	±72
C: 0.1365	-530	-467	±46
D: 0.1985	-220	-126	±23

The neutron diffraction measurements are shown in Table 3. The data in the first column have been obtained by scanning through the material to different depths below the unpolished region A, this means that this data has not been influenced by any possible stress redistribution which may have resulted from the electro-polishing process. Further identical neutron diffraction residual stress measurements were made at locations B, C and D, as reported by Bonner *et al* [3]. These values are also presented in Table 3, and show some difference in the residual stress values measured at the equivalent depth as those made at position A.

Table 3. Residual stress values from neutron diffraction measurements

Location and depth (mm)	Residual Stress, MPa			
	A	B	C	D
A: 0.0528	-920.5			
B: 0.1312	-642	-646		
C: 0.1636	-378.5		-369	
D: 0.2329	-54			-31

In this case, with a relatively thick specimen geometry, the results show that stress redistribution appears to be more pronounced at greater depths of material removal. This is further illustrated in Figure 3, which shows the change in the residual stress values expressed as percentages using the following methods for the XRD and the neutron diffraction data:

XRD – the percentage change in this case is the difference between the 'raw' and the 'corrected' data expressed as a percentage of the original 'raw' data value.

ND – the percentage change in this case is the difference between the data measured at location A and the values measured at the electro-polished locations B, C and D. This difference is expressed as a percentage of the value measured at location A.

Fig. 7. shows that for shallow depth increments of material removal the percentage change in the residual stress values for the XRD and neutron methods are of a similar magnitude, around 5 to 10%. With increasing depth the residual stresses approach zero (this occurs at around 0.25 mm from Figure 8), so any error in the measured stress value caused by redistribution has a more significant effect on the measurement accuracy and uncertainty. The last data point in Figure 7 illustrates this and consequently is somewhat misleading. Since there were no XRD measurements conducted at this depth it is unclear as to the effect on the XRD data.

The results are plotted against depth in Figure 8. This Figure presents the corrected XRD data plotted for comparison with the neutron diffraction data and associated error measured at the four electro-polished locations.

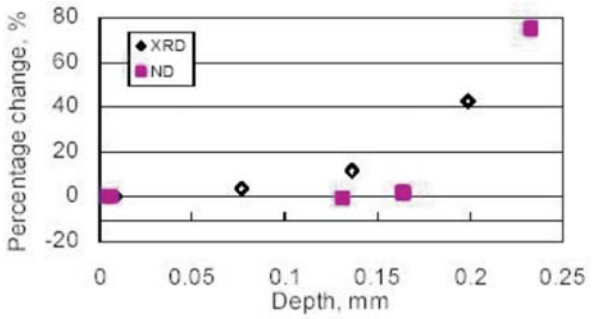

Fig. 7. Percentage change in the residual stress value caused by corrections (XRD) or stress redistribution (ND)

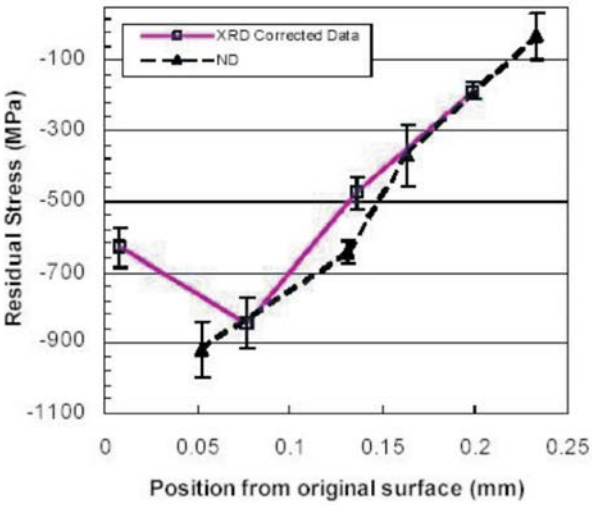

Fig. 8. Comparison of XRD and ND (Pos A, B, C and D for yttria stabilized zirconia coatings) near surface stress measurements

VII. CONCLUSION

Through comparison it has been shown that residual stress measurements obtained using X-ray diffraction

techniques are in good agreement with results obtained by neutron diffraction. Although the correction seems minor given the magnitude of the stresses, it does provide improved measurement accuracy. Interestingly, apart from the deviation in the neutron data at a depth of 0.1312 mm there is linear trend in the stress profile as material is removed, which is also evident in the XRD data in fig 8.

REFERENCES

[1] L. Pawlowski, 1995, "The Science and Engineering of Thermal Spray Coatings", Wiley.

[2] M.I. Boulos, P. Fauchais, E. Pfender, 1994, "Thermal Plasmas", Plenum Press.

[3] Withers PJ, Bhadeshia HKDH, 2000, "Overview: Residual Stress, Part 1—Measurement Techniques", Materials Science and Technology, 17: 355. http://www.msm.cam.ac.uk/phase-trans/2001/mst4640a.pdf (Accessed: 9.02.2004)

[4] Noyan IC, Cohen JB, 1987, "Residual Stress Measurement by Diffraction and Interpretation", New York: Springer-Verlag.

[5] .M.E. Fitzpatrick, A.T. Fry, P. Holdway, F.A. Kandil, J. Shackleton and L. Suominen, 2002, "NPL Good Practice Guide No. 52: Determination of Residual Stresses by X-ray Diffraction".

Anderson is a research scholar and a Senior Lecturer at the department of mechanical Engineering, Sathyabama University, Chennai. He has over 10 years of teaching experience and his field of research is Surface Engineering.